

GaussNav: Gaussian Splatting for Visual Navigation

Xiaohan Lei¹, Min Wang², Wengang Zhou^{1,2}, and Houqiang Li^{1,2}

¹ University of Science and Technology of China

² Hefei Comprehensive National Science Center

leixh@mail.ustc.edu.cn wangmin@iai.ustc.edu.cn

{zhwg,lihq}@ustc.edu.cn

Project page: <https://xiaohanlei.github.io/projects/GaussNav/>

Abstract. In embodied vision, Instance ImageGoal Navigation (IIN) requires an agent to locate a specific object depicted in a goal image within an unexplored environment. The primary difficulty of IIN stems from the necessity of recognizing the target object across varying view-points and rejecting potential distractors. Existing map-based navigation methods largely adopt the representation form of Bird’s Eye View (BEV) maps, which, however, lack the representation of detailed textures in a scene. To address the above issues, we propose a new Gaussian Splatting Navigation (abbreviated as GaussNav) framework for IIN task, which constructs a novel map representation based on 3D Gaussian Splatting (3DGS) [15]. The proposed framework enables the agent to not only memorize the geometry and semantic information of the scene, but also retain the textural features of objects. Our GaussNav framework demonstrates a significant leap in performance, evidenced by an increase in Success weighted by Path Length (SPL) from 0.252 to 0.578 on the challenging Habitat-Matterport 3D (HM3D) dataset. Our code will be made publicly available.

Keywords: Embodied Visual Navigation · 3D Gaussian Splatting

1 Introduction

As an emerging research topic, Embodied Artificial Intelligence (EAI) has been drawing an increasing interest in the community. This field demands that agents are capable of exploration, learning, reasoning, and interaction within the physical world. A critical question then arises: how can an embodied agent comprehend its world? Recent years have witnessed rapid advancements in radian field technologies, exemplified by the development of Neural Radiance Fields (NeRF) [27] and 3D Gaussian Splatting (3DGS) [15], among others. This leads to the subsequent inquiry: how can we leverage these radian field technologies to facilitate embodied tasks for agents?

To address this question, we focus on the embodied visual navigation [7, 18, 22, 44]. Traditional navigation has been studied over the past years, but with the

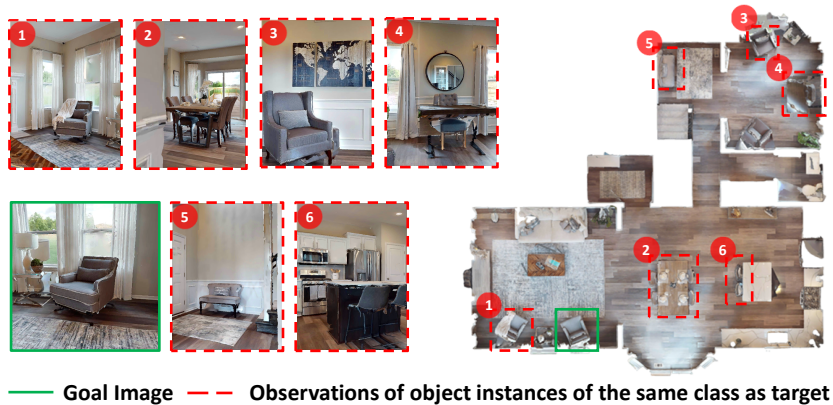


Fig. 1: Instance ImageGoal Navigation (IIN) requires agent to navigate to the object instance depicted in the goal image, while distinguishing it from other visually similar instances of the same class.

advent of deep learning technologies, there is a renewed interest in navigating agents and also understanding the semantic intricacies of the 3D environment. For instance, consider a scenario where an agent is presented with a randomly captured image of a specific object, the agent’s task is to navigate to this object within a certain time budget. To distinguish the target from different angle of views, the agent has to understand the object’s geometry, its semantic attributes, and its spatial relationship to the environment. This task, named as Instance ImageGoal Navigation (IIN) was introduced by Krantz *et al.* [19] for embodied visual navigation, as depicted in Fig. 1.

Recently, map-based visual navigation methods [1,4,5,17,25,29] have focused on constructing explicit episodic Bird-Eye-View (BEV) maps, achieving notable success in established visual navigation benchmarks. These well-designed explicit map representations are memory-efficient, storing essential information such as 2D geometry and semantics, and can be directly utilized to calculate the agent’s subsequent actions. However, this simple 2D BEV map representation is not free from its limitations. For instance, it lacks the capacity to retain 3D geometrical information about the environment, rendering it ineffective for navigating cross-floor scenarios. Additionally, BEV maps are unable to preserve the intricate textures and detailed features in a scene. To address the above issues in existing map-based visual navigation methods, we formulate a new Gaussian Splatting Navigation framework, *i.e.*, GaussNav, for IIN task.

Our GaussNav framework consists of three stages, Sub-gaussians Division, Semantic Gaussian Construction and Gaussian Navigation. First, to address the optimization difficulties of 3DGS in large scenes on computationally constrained devices, we propose dividing gaussians into corresponding sub-gaussians and optimizing each of them individually. Second, we introduce a new form of map representation, *i.e.*, Semantic Gaussian. By leveraging Semantic Segmentation algorithms, we assign semantic labels to each gaussian. We then cluster gaussians with their semantic labels and 3D positions, segmenting objects in the scene

into different instances under various semantic categories. This representation is capable of preserving not only the 3D geometry of the scene and the semantic labels of each gaussian but also the texture details of the scene, thereby enabling novel view synthesis. Third, we render descriptive images for object instances, matching them with the goal image to effectively locate the target object. Upon determining the predicted goal object’s position, we can efficiently transform our Semantic Gaussian into grid map and employ path planning algorithms.

With our proposed method, GaussNav, the difficult IIN task can be transformed into a more tractable PointGoal Navigation task, consequently yielding more promising results. On the challenging Habitat-Matterport 3D dataset (HM3D) [41], we achieve 0.725 success and 0.578 SPL. This represents a significant improvement over the previous state-of-the-art work [21], which reported success of 0.702 and SPL of 0.252.

2 Related Work

We briefly discuss related work on ImageGoal, Instance ImageGoal Navigation (IIN) and 3DGS below.

ImageGoal Navigation. ImageGoal Navigation requires the agent to navigate to the location where the goal image is captured, matching the position and orientation accurately. The goal image is taken with parameters identical to those of the agent’s RGB-D camera, including agent’s height, field-of-view, and image size. To tackle this challenge problem, researchers adopt various strategies. Some optimize RL policy [1, 8, 39, 40] that directly maps observations to actions. Others focus on constructing maps [6, 16, 20, 30], or on developing carefully hand-crafted matching algorithm [35]. While these methods yield promising results in ImageGoal Navigation, they do not entirely address the unique demands of the IIN task.

Instance ImageGoal Navigation. The IIN task introduces distinct challenges compared to the ImageGoal Navigation. First, the goal image in IIN must feature a specific object instance, rather than meaningless large white walls in the ImageGoal Navigation. Second, the parameters used to capture the goal image, do not necessarily match those of the agent’s camera. Therefore, to succeed in IIN, an agent must be adept at identifying the target object among numerous candidates of the same class with goal object and recognizing it from various viewpoints. To address these challenges, Krantz *et al.* [17] develop a general pipeline for aligning the same object from different angle of views, Bono *et al.* [3] present an end-to-end approach in the IIN task, and Lei *et al.* [21] propose a method that mimics human behaviour for verifying objects at a distance. Existing methods focus partly on designing more sophisticated modules [17, 21] and partly on pre-training on pretext tasks [3]. Our approach differs in that we concentrate on designing a new map representation. Through this novel form of map, we can better establish the connection between target descriptions and target locations, thereby facilitating visual navigation.

3D Gaussian Splatting. 3DGS, proposed by Bernhard *et al.* [15], models a 3D scene through anisotropic 3D gaussians. This scene representation demonstrates promising results on both rendering speed and quality. Leveraging these advantages, a growing body of research begins to explore various innovations, including deformable or dynamic gaussians [24, 36, 42], advancements in mesh extraction and physics simulation [10, 11, 38], as well as applications in Simultaneous Localization and Mapping (SLAM) [14, 26, 43]. This surge of interest in the capabilities of 3DGS leads us to consider its potential for embodied visual navigation. Given that the gaussian representation inherently encapsulates explicit scene geometry and the parameters required for rendering, we posit that 3DGS can significantly enhance embodied visual navigation. The explicit nature of the gaussian representation provides a rich, condensed form of environmental data, which can be effectively utilized to inform and guide autonomous agents in navigation.

3 Methods

3.1 Preliminaries

In the IIN task, at the start of a new episode e , the agent is given a goal image I_g that features a specified object instance o . The agent’s task is to navigate to this instance within the environment. At each timestep t , the agent acquires observations which include an RGB image I_t , a depth image D_t , and sensor pose reading P_t . Utilizing this information, the agent must decide upon and execute an action a_t . When calling stop action, the episode is success only if the agent is within a certain range of the goal object.

We propose a modular framework called Gaussian Splatting for Visual Navigation (GaussNav) to tackle the IIN task. In a new environment, the Instance ImageGoal Navigation in our proposed framework consists of three stages: Sub-gaussians Division, as shown in Fig. 2, Semantic Gaussian Construction, as depicted in Fig. 3a, and Gaussian Navigation, illustrated in Fig. 3b. Initially, during the first episode within a unknown environment, the agent employs frontier exploration to explore the environment and collect observations. We first divide the observations into subsets and use our proposed Semantic Gaussian to reconstruct each of the sub-scene. Subsequently, in the following episodes, the agent leverages the Semantic Gaussian to grounding the object instance o depicted in the goal image and navigate to it. This process effectively transforms the IIN task into a more manageable PointGoal Navigation task.

3.2 Sub-gaussians Division

In the first episode of an unexplored environment, the agent simultaneously maintains two types of maps, an exploration map and an obstacle map. The exploration map delineates the regions of the environment that have been explored, while the obstacle map marks the obstacles in the scene. By detecting

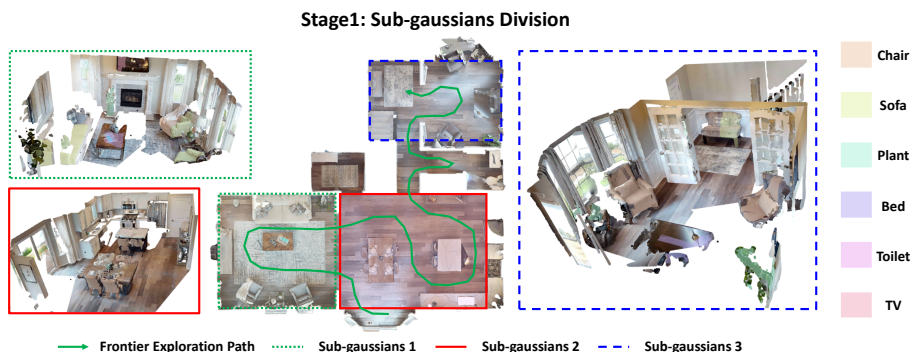


Fig. 2: Sub-gaussians Division. When initialized in an unknown environment, agent first employs frontier exploration to explore the environment. The agent will next partition the collected observations into distinct subsets for constructing sub-gaussians, in preparation for the subsequent Semantic Gaussian Construction.

the contours of the exploration map and excluding areas in the obstacle map, the agent set the closest frontier point as waypoint to facilitate exploration. By the applying frontier-based exploration strategy, the agent collects observations of the entire environment. As depicted in Fig. 2, we divide observations along the trajectory into distinct subsets. Then each subset is used to construct Semantic Gaussian in the next stage of Semantic Gaussian Construction.

3.3 Semantic Gaussian Construction

We formulate our Semantic Gaussian Construction problem as, given a set of camera poses and RGB-D images, construct a semantic gaussian map. The semantic gaussian map can represent scene’s geometry, feature scene’s semantic information and render high-fidelity RGB-D image given an arbitrary camera pose. At any timestep t , the agent’s RGB observation I_t is segmented into C_t using Mask-RCNN [12]. Specifically, C_t is a $6 \times H \times W$ mask, where 6 is the number of possible goal categories in the IIN task. At $t = 0$, the Semantic Gaussian is initialized with a semantically labeled point cloud based on the observed RGB I_0 , depth image D_0 , and segmentation result C_0 . Subsequently, the gaussians are initialized and optimized based on the point cloud. When $t > 0$, Gaussian Densification is performed by comparing the rendered results at position P_t with the ground truth, followed by an update to the semantic Gaussian through differentiable rendering, as depicted in Fig. 3a.

Gaussian Map Representation. The Semantic Gaussian of the scene is represented as a set of semantically labeled gaussians. The representation of gaussians is simplified compared to 3DGS [15] by using only view-independent color and constraining gaussians to be isotropic. Consequently, each gaussian is characterized by a minimal set of eight parameters: a triplet for the RGB color vector \mathbf{c} , a triplet delineating the centroid $\boldsymbol{\mu} \in \mathbb{R}^3$, a scalar representing the radius r , a scalar quantifying the opacity $o \in [0, 1]$, and a scalar representing the

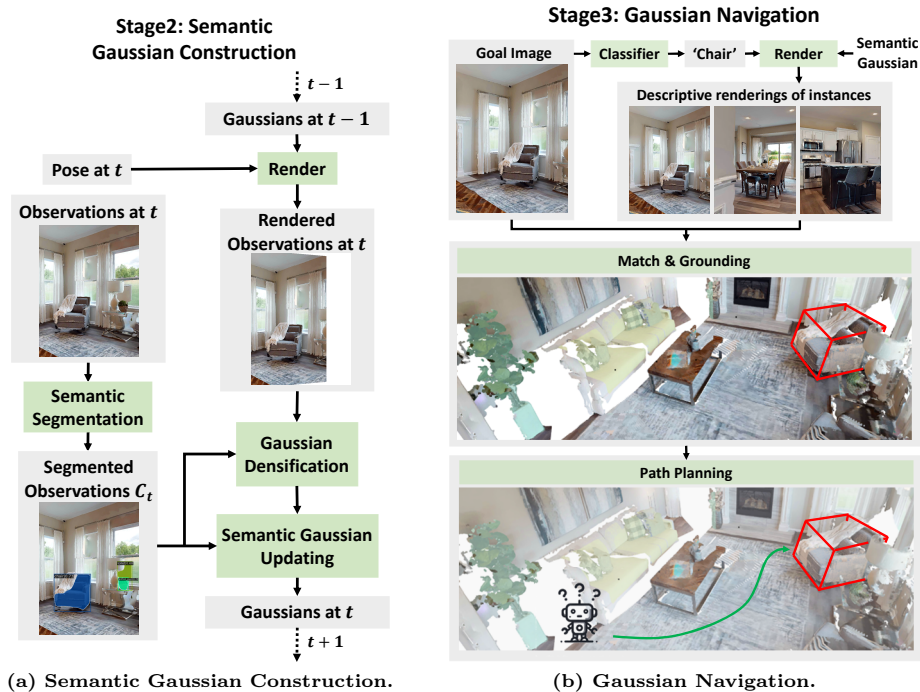


Fig. 3: The last two stages of our GaussNav framework. (a) Semantic Gaussian Construction. At timestep t , the pipeline updates the gaussians from $t - 1$ through densification and updating, which involves a comparison between the rendered RGB and depth images against the current input training views. Concurrently, semantic labels are assigned to the densified gaussians using the segmented images. Finally, the gaussians are refined through differentiable rendering. **(b) Gaussian Navigation.** Our approach begins with the classification of the goal image using pre-constructed Semantic Gaussian. Upon determining the predicted class, we generate descriptive images around instances belonging to that class. These images are then matched with the target object to identify and ground the goal instance. Utilizing the map and the established goal, the agent employs path planning to compute the sequence of actions.

category label l . Each gaussian influences a point in 3D space $\mathbf{x} \in \mathbb{R}^3$ according to the standard unnormalized Gaussian equation weighted by its opacity:

$$f(\mathbf{x}) = o \exp\left(-\frac{\|\mathbf{x} - \boldsymbol{\mu}\|^2}{2\sigma^2}\right). \quad (1)$$

Differentiable Rendering via Splatting. Following the original 3DGS [15], our Semantic Gaussian renders an RGB image as follows: given a collection of 3D gaussians and camera pose, first sort all gaussians from front to back. RGB images can then be efficiently rendered by alpha-compositing the splatted 2D projection of each gaussian in order in pixel space. The rendered color of pixel

$\mathbf{p} = (u, v)$ can be written as:

$$\hat{I}(\mathbf{p}) = \sum_{i=1}^n \mathbf{c}_i f_i(\mathbf{p}) \prod_{j=1}^{i-1} (1 - f_j(\mathbf{p})), \quad (2)$$

where $f_i(\mathbf{p})$ is computed as in Eq. (1) but with $\boldsymbol{\mu}$ and r of the splatted 2D Gaussians in pixel-space:

$$\boldsymbol{\mu}^{2D} = K \frac{E_t \boldsymbol{\mu}}{d}, \quad r^{2D} = \frac{fr}{d}, \quad \text{where } d = (E_t \boldsymbol{\mu})_z. \quad (3)$$

Here, K is the camera’s intrinsic matrix, E_t embodies the extrinsic matrix that encodes the camera’s rotation and translation at time t , f denotes the known focal length, and d is the depth of the i^{th} gaussian relative to the camera’s coordinate frame.

Following Keetha *et al.* [14], we also differentiably render depth and silhouette image, which determines the visibility. The depth image D at pixel \mathbf{p} is rendered as follows:

$$\hat{D}(\mathbf{p}) = \sum_{i=1}^n d_i f_i(\mathbf{p}) \prod_{j=1}^{i-1} (1 - f_j(\mathbf{p})), \quad (4)$$

Similarly, the silhouette image S at pixel \mathbf{p} , which indicates the presence of Semantic Gaussian information, is rendered via:

$$\hat{S}(\mathbf{p}) = \sum_{i=1}^n f_i(\mathbf{p}) \prod_{j=1}^{i-1} (1 - f_j(\mathbf{p})). \quad (5)$$

Above these, we also render the semantic segmentation results as follows:

$$\hat{C}(\mathbf{p}) = \sum_{i=1}^n l_i f_i(\mathbf{p}) \prod_{j=1}^{i-1} (1 - f_j(\mathbf{p})). \quad (6)$$

Gaussian Densification and Updating. Gaussian Densification aims to initialize new gaussians in the Semantic Gaussian at each new incoming frame. Following Keetha *et al.* [14], we add new gaussians based on a densification mask to determine which pixels should be densified:

$$M(\mathbf{p}) = \left(\hat{S}(\mathbf{p}) < 0.5 \right) + \left(D(\mathbf{p}) < \hat{D}(\mathbf{p}) \right) \left(\mathbb{L}_1(\hat{D}(\mathbf{p})) > 50\text{MDE} \right), \quad (7)$$

where the first term represents where the Semantic Gaussian isn’t adequately dense, and the second term indicates where the ground-truth depth is in front of the predicted depth and the depth error is greater than 50 times the median depth error (MDE). After densifying current Semantic Gaussian, we update the parameters of gaussians given poses and observations. This is done by differentiable-rendering and gradient-based-optimization, which is equivalent to the “classic” problem of fitting a radiance field to images with known poses.

3.4 Gaussian Navigation

Once the Semantic Gaussian is constructed and the agent’s initial pose is known, transforming IIN into PointGoal Navigation requires: 1. converting the Semantic Gaussian into a map form that can be used for path planning, *i.e.*, either 3D voxels M_{3D} or 2D BEV grids M_{2D} , and 2. predicting the position of the target object instance \hat{P}_g . Therefore, we first convert the Semantic Gaussian into a point cloud, whereby each gaussian is reduced to a single point in the point cloud representation. The point cloud is then voxelized into 3D voxels M_{3D} , then the 3D voxels M_{3D} are projected to 2D BEV grids M_{2D} . By classifying and matching in the pre-built Semantic Gaussian G_s with goal image I_g , we can ground target object’s position \hat{P}_g , as depicted in Fig. 3b. Given start pose P_0 , predicted target object’s position \hat{P}_g and grid map M_{2D} , we can easily use Fast Marching Method (FMM)³ to compute the shortest path and the corresponding action a_t .

Classifier. In IIN task, the agent receives an image depicting the target object I_g . However, comparing this image with renderings from navigable points within the entire scene becomes exceedingly time-inefficient due to the vastness of the search space. Consequently, with our Semantic Gaussian G_s , we only need to search for instances of the object category corresponding to the goal object. Therefore, we first classify the goal image I_g into target category label \hat{l}_g . We use the goal images on the train split of HM3D-SEM [41] to finetune the image classification model, *i.e.*, ResNet50 [13], pretrained on ImageNet [9].

Match & Grounding. With the predicted target object’s label \hat{l}_g , we identify all candidate objects that share the same class label. For each candidate instance, we generate a set of descriptive images by rendering the object from multiple viewpoints to capture its features. n denotes the observed instances of the same class as target object, S_i indicates the i -th object instance’s descriptive renderings, then the universal set of S can be formulated as:

$$S = \{S_1, S_2, \dots, S_n\} \quad \text{for } i = 1, 2, \dots, n. \quad (8)$$

To distinguish the target object from these candidates, we can formulate the question as:

$$i_{\max} = \arg \max \left\{ \max_{s \in S_1} K(s), \max_{s \in S_2} K(s), \dots, \max_{s \in S_n} K(s) \right\} \quad \text{for } i = 1, 2, \dots, n, \quad (9)$$

where $K(\cdot)$ is defined as the matched number of keypoints between renderings and goal image I_g . Specifically, we extract the pixel-wise (x, y) coordinates of the keypoints and their associated feature descriptors using DISK [33] both on RGB renderings and goal image. Subsequently, the matched pairs are computed using LightGlue [23]. The candidate object whose rendered images yield the highest number of matched keypoints is then selected as the target object, as in Eq. (9).

When the object instance is selected, we ground the object both in the 3D voxels M_{3D} and 2D BEV grid map M_{2D} . Due to the presence of outliers in

³ <https://pythonhosted.org/scikit-fmm/>

the projection of an object instance onto the 2D BEV map, which are caused by errors in semantic segmentation, we perform clustering on the instances on the map. Specifically, we use Density-based Spatial Clustering of Applications with Noise (DBSCAN)⁴, which groups together points that are closely packed together, marking as outliers points that lie alone in low-density regions. With the precise selected object instance’s location, we can easily transform the IIN task to a PointGoal task.

Path Planning. Given 2D BEV grid map M_{2D} , along with the agent’s starting position and the goal’s location, we can efficiently generate a shortest distance field using FMM. Each point within this field encapsulates the minimal distance necessary to traverse from the starting point to the goal. We extract a relevant subset of this distance field that falls within the agent’s operational range. Subsequently, a waypoint is chosen from this subset to ensure it avoids any intersections with obstacles while adhering to a local minimum in the distance field. With the selected waypoint, the agent can readily calculate an action based on the angle and distance from its current state. The agent iterates the aforementioned process to generate a sequence of actions, continuing until the destination is reached.

4 Experiments

4.1 Experiment Setup

Datasets. We use Habitat-Matterport 3D dataset (HM3D) [41] in the Habitat [32] for our experiments. HM3D consists of scenes which are 3D reconstructions of real-world environments with semantic annotations. These scenes are split into three distinct subsets for training, validation, and testing, consisting of 145/36/35 scenes, respectively. We follow the task setting of Instance Image-Goal Navigation (IIN) proposed by Krantz *et al.* [19]. The episode dataset has been partitioned into three subsets for training, validation, testing, comprising 7,056K/1K/1K episodes respectively. The object depicted by the goal image belongs to the following six categories: {“chair”, “couch”, “plant”, “bed”, “toilet”, “television”}. On the validation subset, a total of 795 unique object instances have been observed.

Embodiment. We adopt the embodiment parameters from the Hello Robot Stretch platform⁵. The simulated agent is modeled as a rigid-body cylinder with zero turning radius, a height of 1.41m, and a radius of 0.17m. A forward-facing RGB-D camera is affixed at a height of 1.31 m. At each timestep t , the agent’s observation consists of an egocentric RGB image, depth image, goal image and sensor pose reading. Camera specifications, such as mounting height, look-at angle, and field of view (FOV), differ between the agent’s and the goal’s cameras.

⁴ <https://scikit-learn.org/stable/modules/generated/sklearn.cluster.DBSCAN.html>

⁵ <https://hello-robot.com/stretch-2>

Table 1: Performance of our proposed GaussNav as compared to the baselines and previous state-of-the-art methods on the HM3D [41] datasets across two different metrics: Success and SPL [2].

Method	Success \uparrow	SPL \uparrow
RL Baseline [19]	0.083	0.035
OVRL-v2 ImageNav [39]	0.006	0.002
OVRL-v2 IIN [39]	0.248	0.118
Mod-IIN [17]	0.561	0.233
IEVE Mask RCNN [21]	0.684	0.241
IEVE InternImage [21]	0.702	0.252
GaussNav (ours)	0.725	0.578

Specifically, the agent’s camera resolution is 640×480 , whereas the goal’s camera has a resolution of 512×512 with unfixed height and FOV parameters.

Action Space. We use a discrete action space for navigation, comprising four actions: {STOP, FORWARD, TURN_RIGHT, TURN_LEFT}. The STOP action terminates the current episode, while the FORWARD action advances the agent by 25 cm. Rotational actions occur in place: TURN_RIGHT induces a 25-degree clockwise rotation and TURN_LEFT a 25-degree counter-clockwise rotation.

Evaluation Metrics. We evaluate our model with both success and efficiency. We report Success Rate (Success), Success rate weighted by normalized inverse Path Length (SPL). An episode is deemed successful (Success = 1) if the agent invokes the STOP action within a 1.0m Euclidean distance from the goal object. SPL is an efficiency measure defined in [2], is given by:

$$\text{SPL} = \frac{1}{N} \sum_{i=1}^N S_i \cdot \frac{l_i}{\max(p_i, l_i)}, \quad (10)$$

where N is the total number of episodes, S_i is a binary success indicator for episode i , l_i is the shortest path distance from the start position to the goal, and p_i is the path length actually traversed by the agent. A higher SPL value indicates more efficient navigation.

4.2 Comparison to the state-of-the-art methods

We evaluate our proposed model against various baselines and previous state-of-the-art work, as presented in Tab. 1.

RL Baseline. The baseline model for the IIN task is trained end-to-end using Proximal Policy Optimization (PPO). Training is conducted from scratch as described by Schulman *et al.* [31]. Despite requiring a substantial 3.5 billion steps for the RL agent to converge, the ability to generalize to unseen scenes is lacking (row 1 in Tab. 1).

OVRL-v2 Baseline. Offline Visual Representation Learning v2 (OVRL-v2) was introduced by Karmesh et al. [39]. This novel approach to model-free,

end-to-end navigation policies underscores the importance of self-supervised pre-training for visual encoders and presents the innovation of a Compression Layer (CL). Originally, OVRL-v2 was trained for the ImageGoal Navigation task. Direct application of OVRL-v2 to IIN task without fine-tuning yields suboptimal performance, as indicated by a Success of 0.006 (row 2 in Tab. 1). This reduced efficacy can be attributed to several factors: the transition between scene datasets from Gibson [37] to HM3D [41], differences in robot embodiment from Locobot ⁶ to Stretch, and a shift in the nature of goal destinations from image sources to image subjects. Fine-tuning OVRL-v2 specifically for IIN task on the HM3D dataset significantly improves outcomes, resulting in a Success of 0.248 (row 3 in Tab. 1).

Mod-IIN. Mod-IIN [17] presents a decomposition of the IIN task into four sub-tasks: exploration, goal instance re-identification, goal localization, and local navigation. This method utilizes feature matching to re-identify the goal instance within the egocentric vision and projects the matched features onto a map to localize the goal. Each sub-task is addressed using off-the-shelf components that do not require any fine-tuning. It achieves a Success of 0.561 and SPL of 0.233 (row 4 in Tab. 1).

IEVE. The IEVE approach [21] is inspired by the human heuristic of “getting closer to confirm” when attempting to distinguish objects from a distance. IEVE adopts a modular architecture that enables dynamic switching between exploration, verification, and exploitation actions. This flexibility empowers the agent to make informed decisions tailored to varying circumstances. Results demonstrate that IEVE, when integrated with Mask RCNN [12], achieves Success of 0.684 and an SPL of 0.241, as well as Success of 0.702 and SPL of 0.252 (rows 5 and 6 in Tab. 1) when using InternImage [34].

GaussNav (ours). GaussNav demonstrates a significant performance advantage over all baseline models (row 7 in Tab. 1). It significantly surpasses all existing models in terms of SPL by a huge margin of 0.326 (rows 6 and 7 in Tab. 1). We attribute the superior performance of our method to the direct mapping from goal image to goal position, thereby facilitating efficient navigation without additional exploration. In its initial episode within a new scene, agent explores and construct the Semantic Gaussian of the scene. Semantic Gaussian enables agent to efficiently and accurately locate the goal’s location in following episodes.

4.3 Ablation Study

To understand the modules of our GaussNav, we consider the following ablations:

GaussNav w.o. Classifier. In Fig. 3b, we replace the Classifier’s output with a random generated target category. We observe that the Success drops to 0.375 and the SPL decreases to 0.291 (row 2 in Tab. 2). This is because correct classification is a prerequisite for our method to filter potential candidates.

⁶ <http://www.locobot.org/>

Table 2: Ablations. Table showing comparison of our proposed model, GaussNav, with ablations and ground truth goal position and Match on HM3D dataset.

Ablations	Success \uparrow	SPL \uparrow
GaussNav	0.725	0.578
GaussNav w.o. Classifier	0.375	0.291
GaussNav w.o. Match	0.444	0.353
GaussNav w. SIFT	0.655	0.519
GaussNav w. GlueStick [28]	0.723	0.577
GaussNav w. GT Match	0.850	0.672
GaussNav w. GT Goal Localization	0.946	0.744

Table 3: Number of object instances. The table displays the number of object instances across different categories in the first floor of scene CrMo8WxCyVb.

Chair	Sofa	TV	Plant	Toilet	Bed
11	2	1	3	1	0

GaussNav w.o. Match. The Match module is designed to distinguish target from candidates with the same class. Without the Match module, we randomly select from these candidates. The Success and SPL falls to 0.444 and 0.353 (row 3 in Tab. 2). This can be attributed to the random selection of candidate instances without Match module.

GaussNav w. SIFT or GlueStick [28]. To evaluate the impact of different extractors and matching algorithms on our GaussNav, we replace the combination of DISK [33] + LightGlue [23]. We employ both SIFT + FLANN and GlueStick [28] as alternatives. The first replacement represents a greater decrease, (row 4 in Tab. 2) and the second only displays a slight decrease (row 5 in Tab. 2). These results demonstrate the varying performance of different local feature matching algorithms on the HM3D dataset.

4.4 Efficiency Analysis

Locating the target object within the map is a critical component of our method, which leverages renderings to match and ground the goal object effectively. A naive approach that entails comparing all possible observations at each navigable viewpoint is computationally prohibitive. To address this challenge, we introduce an optimization that constructs semantic gaussians, allowing us to group object instances under their corresponding semantic labels.

Our method significantly reduces the overhead by limiting the comparisons to several descriptive renderings of each instance, rather than searching the entire space. For instance, consider the scene CrMo8WxCyVb-floor-2.9. The navigable area on the first floor of this scene is quantified to be $54.03m^2$. This space can be discretized into approximately 54 squares, each with an area of $1m^2$. Positioned within each square, the agent can observe its surroundings from 12 distinct viewing angles, covering a full 360 deg with each angle spanning 30 deg. Thus,

the original search space for this single floor would consist of $12 \times 54 = 648$ potential observations.

By applying our grouping strategy based on semantic labeling, the search space is considerably narrowed. We count the number of different categories of object instances within the `CrMo8WxCyVb-floor-2.9` scene, as demonstrated in Tab. 3. To locate a “chair” — assuming we render each object instance from three unique viewpoints — the resulting search space is reduced to merely $3 \times 11 = 33$ observations. We render three observations of a single instance to ensure rendering quality, which is achievable only when the new viewpoint largely overlaps with the training views. This optimization yields a significant improvement in time efficiency.

4.5 Error Analysis

The performance of the proposed model is still far from perfect. We would like to understand the error modes for future improvements. Our analysis identifies two sources of error: the first being the model’s inability to consistently match the target from instance renderings, and the second, inaccuracies in goal localization. To quantify the impact of these error sources, we conduct an evaluation of our model using a ground truth Match module and an accurate goal localization. The first one means agent can correctly recognize the target from candidate observations, and the second suggests agent is directly provided with the ground truth goal position. The variant equipped with a ground truth Match module (**GaussNav w. GT Match** in Tab. 2) shows that Success can be enhanced by approximately 0.127 (rows 5 and 6 in Tab. 2). Furthermore, when the model is augmented with both ground truth Match and Goal Localization, denoted as **GaussNav w. GT Goal Localization**, we observe an increase in Success from 0.850 to 0.946, as indicated in rows 6 and 7 in Tab. 2. Improvements in the first error source may be achievable through the development of a more robust re-identification algorithm. As for the second source, a more precise Grounding strategy could yield better results. These insights not only highlight the model’s current shortcomings but also chart a course for subsequent refinement efforts.

4.6 Gaussian Construction Results

In Fig. 4, we present an evaluation of the rendering quality produced by our Semantic Gaussian Construction method on the HM3D validation dataset [41]. To align with the constraints of IIN task [19], we divide each scene within HM3D into separate floors and restrict the agent’s movement to within a single floor, as the IIN task [19] inherently ensures that both the agent’s starting location and the target’s position are on the same floor.

To quantitatively analyze the results in Fig. 4, we observe that the rendering results exhibit a bifurcated trend. For instance, in scenes with indices 29 and 30, the rendered images achieve a high PSNR of up to 40 and a near-zero depth rendering error. However, the rendering performance for scene 10 is sub-optimal. We hypothesize that this polarized rendering quality across different

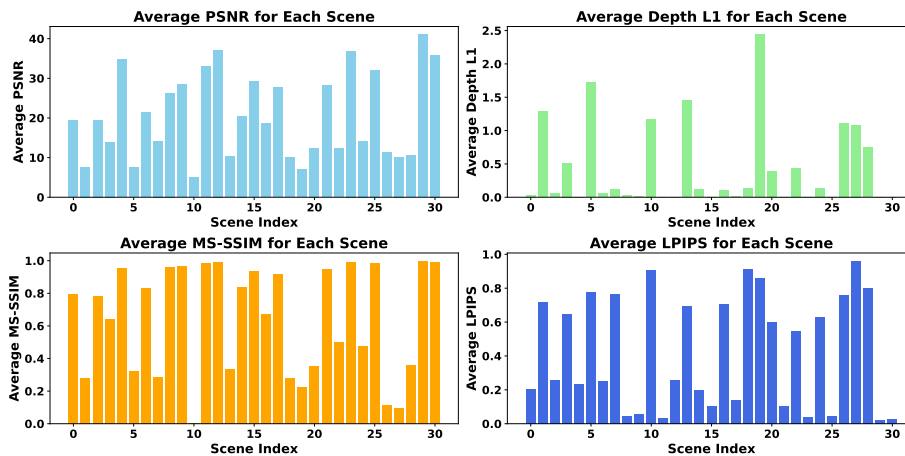


Fig. 4: Rendering quality of our Semantic Gaussian Construction results on the HM3D validation dataset. The x-axis indicates different scene indices with the corresponding floor height.



Fig. 5: Observations rendered from HM3D [41] scene dataset using the Habitat [32] simulator.

scenes can be attributed to the discrepancy between the simulation and reality. This is evident in Fig. 5, where some renderings from the HM3D dataset using Habitat simulator exhibit low fidelity, particularly in highly textured environments. High-quality reconstruction in such intricate settings is difficult, and utilizing suboptimal renderings as a basis for 3D environment reconstruction can further degrade the quality of the final output. In light of this, for scenes that are poorly reconstructed, we maintain consistency by using the original training views, rather than attempting to render novel views which would likely result in a diminished quality.

5 Conclusion

In this work, we introduce a modular approach for visual navigation, *i.e.*, Gaussian Splatting for Visual Navigation (GaussNav). Previous map-based methods largely focus on building 2D BEV map, which cannot represent the 3D geometry and detailed features in a scene. To this end, we propose a novel map

representation, Semantic Gaussian, which is capable of preserving the scene’s 3D geometry, semantic labels associated with each Gaussian, and intricate texture details. Leveraging this novel representation of map, we directly predict the position of target object depicted in the goal image, thereby transforming IIN into a more tractable PointGoal Navigation task. Our proposed model achieves state-of-the-art performance, significantly enhancing SPL from 0.252 to 0.578. Furthermore, we analyze the error modes for our model and quantify the scope for improvement along two important dimensions (match and object grounding) in the future work.

References

1. Al-Halah, Z., Ramakrishnan, S.K., Grauman, K.: Zero experience required: Plug & play modular transfer learning for semantic visual navigation. In: IEEE/CVF Conference on Computer Vision and Pattern Recognition (CVPR). pp. 17031–17041 (2022)
2. Anderson, P., Chang, A., Chaplot, D.S., Dosovitskiy, A., Gupta, S., Koltun, V., Kosecka, J., Malik, J., Mottaghi, R., Savva, M., et al.: On evaluation of embodied navigation agents. arXiv preprint arXiv:1807.06757 (2018)
3. Bono, G., Antsfeld, L., Chidlovskii, B., Weinzaepfel, P., Wolf, C.: End-to-end (instance)-image goal navigation through correspondence as an emergent phenomenon. arXiv preprint arXiv:2309.16634 (2023)
4. Chaplot, D.S., Gandhi, D., Gupta, S., Gupta, A., Salakhutdinov, R.: Learning to explore using active neural slam. arXiv preprint arXiv:2004.05155 (2020)
5. Chaplot, D.S., Gandhi, D.P., Gupta, A., Salakhutdinov, R.R.: Object goal navigation using goal-oriented semantic exploration. *Advances in Neural Information Processing Systems (NeurIPS)* **33**, 4247–4258 (2020)
6. Chaplot, D.S., Salakhutdinov, R., Gupta, A., Gupta, S.: Neural topological slam for visual navigation. In: IEEE/CVF Conference on Computer Vision and Pattern Recognition (CVPR) (June 2020)
7. Cheng, W., Dong, X., Khan, S., Shen, J.: Learning disentanglement with decoupled labels for vision-language navigation. In: *European Conference on Computer Vision (ECCV)*. pp. 309–329. Springer (2022)
8. Choi, Y., Oh, S.: Image-goal navigation via keypoint-based reinforcement learning. In: *International Conference on Ubiquitous Robots (UR)*. pp. 18–21 (2021)
9. Deng, J., Dong, W., Socher, R., Li, L.J., Li, K., Fei-Fei, L.: Imagenet: A large-scale hierarchical image database. In: IEEE/CVF Conference on Computer Vision and Pattern Recognition (CVPR). pp. 248–255 (2009)
10. Feng, Y., Feng, X., Shang, Y., Jiang, Y., Yu, C., Zong, Z., Shao, T., Wu, H., Zhou, K., Jiang, C., Yang, Y.: Gaussian splashing: Dynamic fluid synthesis with gaussian splatting. arXiv preprint arXiv:2401.15318 (2024)
11. Guédon, A., Lepetit, V.: Sugar: Surface-aligned gaussian splatting for efficient 3d mesh reconstruction and high-quality mesh rendering. arXiv preprint arXiv:2311.12775 (2023)
12. He, K., Gkioxari, G., Dollár, P., Girshick, R.: Mask r-cnn. In: IEEE/CVF Conference on Computer Vision and Pattern Recognition (CVPR). pp. 2961–2969 (2017)
13. He, K., Zhang, X., Ren, S., Sun, J.: Deep residual learning for image recognition. arXiv preprint arXiv:1512.03385 (2015)

14. Keetha, N., Karhade, J., Jatavallabhula, K.M., Yang, G., Scherer, S., Ramanan, D., Luiten, J.: Splatam: Splat, track & map 3d gaussians for dense rgb-d slam. arXiv preprint arXiv:2312.02126 (2023)
15. Kerbl, B., Kopanas, G., Leimkühler, T., Drettakis, G.: 3d gaussian splatting for real-time radiance field rendering. *ACM Transactions on Graphics* **42**(4) (July 2023)
16. Kim, N., Kwon, O., Yoo, H., Choi, Y., Park, J., Oh, S.: Topological Semantic Graph Memory for Image Goal Navigation. In: *Conference on Robot Learning (CoRL)* (2022)
17. Krantz, J., Gervet, T., Yadav, K., Wang, A., Paxton, C., Mottaghi, R., Batra, D., Malik, J., Lee, S., Chaplot, D.S.: Navigating to objects specified by images. arXiv preprint arXiv:2304.01192 (2023)
18. Krantz, J., Lee, S.: Sim-2-sim transfer for vision-and-language navigation in continuous environments. In: *European Conference on Computer Vision (ECCV)*. pp. 588–603. Springer (2022)
19. Krantz, J., Lee, S., Malik, J., Batra, D., Chaplot, D.S.: Instance-specific image goal navigation: Training embodied agents to find object instances. arXiv preprint arXiv:2211.15876 (2022)
20. Kwon, O., Park, J., Oh, S.: Renderable neural radiance map for visual navigation. In: *IEEE/CVF Conference on Computer Vision and Pattern Recognition (CVPR)*. pp. 9099–9108 (June 2023)
21. Lei, X., Wang, M., Zhou, W., Li, L., Li, H.: Instance-aware exploration-verification-exploitation for instance imagegoal navigation. In: *IEEE/CVF Conference on Computer Vision and Pattern Recognition (CVPR)* (2024)
22. Lin, C., Jiang, Y., Cai, J., Qu, L., Haffari, G., Yuan, Z.: Multimodal transformer with variable-length memory for vision-and-language navigation. In: *European Conference on Computer Vision (ECCV)*. pp. 380–397. Springer (2022)
23. Lindenberger, P., Sarlin, P.E., Pollefeys, M.: Lightglue: Local feature matching at light speed. arXiv preprint arXiv:2306.13643 (2023)
24. Luiten, J., Kopanas, G., Leibe, B., Ramanan, D.: Dynamic 3d gaussians: Tracking by persistent dynamic view synthesis. arXiv preprint arXiv:2308.09713 (2023)
25. Ma, B., Yin, X., Wu, D., Shen, H., Ban, X., Wang, Y.: End-to-end learning for simultaneously generating decision map and multi-focus image fusion result. *Neurocomputing* **470**, 204–216 (2022)
26. Matsuki, H., Murai, R., Kelly, P.H.J., Davison, A.J.: Gaussian splatting slam. arXiv preprint arXiv:2312.06741 (2023)
27. Mildenhall, B., Srinivasan, P.P., Tancik, M., Barron, J.T., Ramamoorthi, R., Ng, R.: Nerf: Representing scenes as neural radiance fields for view synthesis. In: *European Conference on Computer Vision (ECCV)* (2020)
28. Pautrat, R., Suárez, I., Yu, Y., Pollefeys, M., Larsson, V.: GlueStick: Robust image matching by sticking points and lines together. In: *International Conference on Computer Vision (ICCV)* (2023)
29. Ramakrishnan, S.K., Chaplot, D.S., Al-Halah, Z., Malik, J., Grauman, K.: Poni: Potential functions for objectgoal navigation with interaction-free learning. In: *IEEE/CVF Conference on Computer Vision and Pattern Recognition (CVPR)*. pp. 18890–18900 (2022)
30. Savinov, N., Dosovitskiy, A., Koltun, V.: Semi-parametric topological memory for navigation. arXiv preprint arXiv:1803.00653 (2018)
31. Schulman, J., Wolski, F., Dhariwal, P., Radford, A., Klimov, O.: Proximal policy optimization algorithms. arXiv preprint arXiv:1707.06347 (2017)

32. Szot, A., Clegg, A., Undersander, E., Wijmans, E., Zhao, Y., Turner, J., Maestre, N., Mukadam, M., Chaplot, D.S., Maksymets, O., et al.: Habitat 2.0: Training home assistants to rearrange their habitat. *Advances in Neural Information Processing Systems (NeurIPS)* **34**, 251–266 (2021)
33. Tyszkiewicz, M., Fua, P., Trulls, E.: Disk: Learning local features with policy gradient. In: *Advances in Neural Information Processing Systems (NeurIPS)*. vol. 33, pp. 14254–14265 (2020)
34. Wang, W., Dai, J., Chen, Z., Huang, Z., Li, Z., Zhu, X., Hu, X., Lu, T., Lu, L., Li, H., et al.: Internimage: Exploring large-scale vision foundation models with deformable convolutions. *arxiv 2022*. arXiv preprint arXiv:2211.05778 (2023)
35. Wasserman, J., Yadav, K., Chowdhary, G., Gupta, A., Jain, U.: Last-mile embodied visual navigation. In: *Conference on Robot Learning (CoRL)* (2022)
36. Wu, G., Yi, T., Fang, J., Xie, L., Zhang, X., Wei, W., Liu, W., Tian, Q., Xinggang, W.: 4d gaussian splatting for real-time dynamic scene rendering. arXiv preprint arXiv:2310.08528 (2023)
37. Xia, F., Zamir, A.R., He, Z., Sax, A., Malik, J., Savarese, S.: Gibson env: Real-world perception for embodied agents. In: *IEEE/CVF Conference on Computer Vision and Pattern Recognition (CVPR)*. pp. 9068–9079 (2018)
38. Xie, T., Zong, Z., Qiu, Y., Li, X., Feng, Y., Yang, Y., Jiang, C.: Physgaussian: Physics-integrated 3d gaussians for generative dynamics. arXiv preprint arXiv:2311.12198 (2023)
39. Yadav, K., Majumdar, A., Ramrakhya, R., Yokoyama, N., Baevski, A., Kira, Z., Maksymets, O., Batra, D.: Ovr1-v2: A simple state-of-art baseline for imagenav and objectnav. arXiv preprint arXiv:2303.07798 (2023)
40. Yadav, K., Ramrakhya, R., Majumdar, A., Berges, V.P., Kuhar, S., Batra, D., Baevski, A., Maksymets, O.: Offline visual representation learning for embodied navigation. In: *Workshop on Reincarnating Reinforcement Learning at ICLR 2023* (2023)
41. Yadav, K., Ramrakhya, R., Ramakrishnan, S.K., Gervet, T., Turner, J., Gokaslan, A., Maestre, N., Chang, A.X., Batra, D., Savva, M., et al.: Habitat-matterport 3d semantics dataset. In: *IEEE/CVF Conference on Computer Vision and Pattern Recognition (CVPR)*. pp. 4927–4936 (2023)
42. Yang, Z., Gao, X., Zhou, W., Jiao, S., Zhang, Y., Jin, X.: Deformable 3d gaussians for high-fidelity monocular dynamic scene reconstruction. arXiv preprint arXiv:2309.13101 (2023)
43. Yugay, V., Li, Y., Gevers, T., Oswald, M.R.: Gaussian-slam: Photo-realistic dense slam with gaussian splatting. arXiv preprint arXiv:2312.10070 (2023)
44. Zhang, S., Li, W., Song, X., Bai, Y., Jiang, S.: Generative meta-adversarial network for unseen object navigation. In: *European Conference on Computer Vision (ECCV)*. pp. 301–320. Springer (2022)